P 2.89 THE ENHANCED Z_{DR} SIGNATURE IN STRATIFORM CLOUDS ABOVE MELTING LAYER

Jelena Andric[(1)]*, Dusan Zrnic[(2)], Jerry M. Straka[(3)], and Valery Melnikov[(1)]
(1) Cooperative Institute for Mesoscale Meteorological Studies, University of Oklahoma, Norman, Oklahoma
(2) NOAA/OAR National Severe Storm Laboratory, Norman, Oklahoma
(3) University of Oklahoma, Norman, Oklahoma

1. INTRODUCTION

Short centimeter and mm-wavelength radars are well suited for remote observation of clouds. These wavelengths are more sensitive to small cloud particles. Applications include continuously running mm-wavelength Cloud Radars (MMCR), operated by the Atmospheric Radiation Measurement (ARM) program. These radars have vertically pointed beams and thus provide height profiles of cloud parameters above the radars

5- and 10-cm wavelength radars are used to measure precipitation. Development of precipitation cannot be understood without studying cloud processes. Thus, dual-polarization precipitation radars are becoming a choice instrument for measurements of cloud parameters. NOAA's research and development polarimetric radar KOUN employs a polarimetric mode with simultaneous transmission and reception of horizontally (H) and vertically (V) polarized waves (Zrnic et al., 2006). In addition to the standard radar moments, KOUN routinely measures the following polarimetric variables: 1) differential reflectivity, 2) the differential phase, and 3) copolar correlation coefficient (e.g., Doviak and Zrnic, 1993, section 6.8).

The shape of cloud ice crystals is one of the main parameters determined by a growth regime thus obtaining information on the particles' shapes is important. The shapes of ice particles can be estimated with polarimetric radar techniques. Matrosov et al. (1996, 2001) and Reinking et al. (2002) obtained the shapes of cloud particles using depolarization measurements at 3-cm wavelength.

*Corresponding author address:
Jelena Andric, University of Oklahoma, Norman, OK 73072;
e-mail: jelena.andric@noaa.gov

Vivekanadan et al. (1994) demonstrated how polarimetric radar can be used to characterize clouds containing ice crystals by using more than one polarimetric variable. They have shown that Z_h, Z_{DR} and K_{DP} (differential propagation phase) can qualitatively be used for identification of oriented ice crystals and transformation of crystals into aggregates.
Hogan et al. (2002) investigated microphysical characteristics of a stratiform cloud using simultaneous aircraft and polarimetric radar measurements. They suggested that the discrepancy between observed high concentration of small ice crystals and the expected concentration by nucleation process can be explained with secondary ice production by Hallett-Mossop multiplication. Observed high Z_{DR} in the middle of the cloud was attributed by Hogan et al. (2002) to embedded convection and was related to presence of supercooled liquid water which is necessary for riming. Within temperature interval from -3 to -8°C, in riming conditions, if droplets of ~24 μm are present, the Hallett-Mossop multiplication can take place and contribute to increased concentration of ice crystals. Then in the supersaturated conditions, large pristine crystals are formed by the dominant growth process, i.e., vapor deposition.

Information on ice crystals habits is obtained via aircraft observation. Also, laboratory experiments using cloud chambers have provided valuable information regarding ice crystals shape, size and growth, (Magono and Lee, 1966, Pruppacher and Klett, 1980, Bailey and Hallett, 2009). Recently radar polarimetric data have been used to get information on crystal habits. We explore a possibility of using differential reflectivity, measured by S-band radar (10-cm wavelength), to infer the shapes of cloud particles. Differential reflectivity (Z_{DR}) fields in clouds exhibit patterns with "pockets" and layers of high and low values demonstrating the complexity of cloud processes.

The main focus of this paper is on the nature of localized regions of enhanced differential reflectivity that are observed at heights with subfreezing temperatures. Our radar observations show that there can be one or two layer-like or pocket-like regions above the melting layer that have large Z_{DR}. We use a one-dimensional microphysical model in order to explain which crystal habits and growth process contributed most to the observed radar signature. A microphysical model is used for calculation of radar variables and the profiles of these are compared with the observed Z_h and Z_{DR}.

2. OBSERVATIONS

2.1 Synoptic situation

An upper level trough, with an intense jet stream (over 62 ms^{-1}) crossing over Oklahoma, provided favorable dynamical conditions for convective-type mixed winter precipitation. A cold front passed Oklahoma the previous day, so this was a post frontal situation with the cloud system moving from the northwest.

The radar data was obtained near midnight according to UTC time, so we are using the morning sounding from Norman, Oklahoma on 28 January 2009 at 00 UTC for temperature and saturation profile, Fig. 1. Cloud top was at approximately 7.3 km, and temperature at that level was -26ºC. There were two levels, close to each other (upper one is at ~2.2 km, lover at ~1.4 km) at 0ºC temperature. Subfreezing temperatures in the lowest portion of the troposphere (below 1.4 km) and a layer of warmer air (with temperature slightly above 0ºC) above and below the freezing level caused sleet and freezing rain in some areas. Relative humidity with respect to water ranged from 80% (at ~5 km) to 100% (fat ~3 km), indicating that the atmosphere was supersaturated with respect to ice throughout the most of the observed cloud.

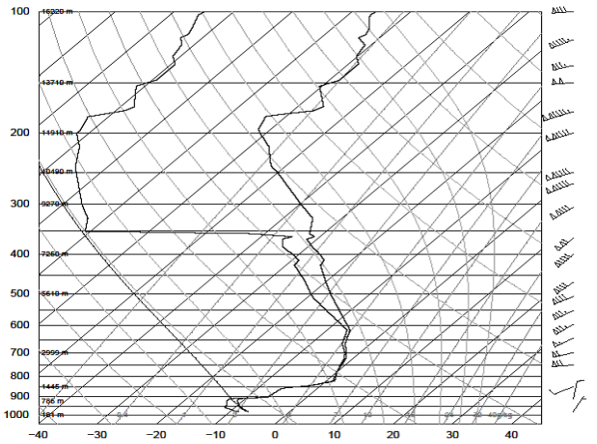

Fig.1. OUN sounding at 28 January 2009, 00Z.

2.2 Observed polarimetric data

WSR-88D KOUN radar employs a polarimetric mode with simultaneous transmission and reception of horizontally and vertically polarized waves. Signals from stratiform clouds are often weak, and thus noise influence on polarimetric variables can be strong. To mitigate noise impact at low SNR, the covariance estimators of polarimetric variables were applied to the time series data from the KOUN (Melnikov and Zrnic, 2007).

Radar data were collected at azimuth 181° and are presented as vertical cross-sections, RHI (Range Height Indicator). Vertical cross-sections of Z_h and Z_{DR}, obtained on 27 January 2009 at 2317 UTC are given in Fig. 2. Our focus is the nature of polarimetric signature above the melting layer.

Enhanced values of Z_h (approximately 45 dBZ) show location of the melting layer between 40 km and ~80 km from the radar and at height level ~2 km. Reflectivity factor alone does not provide much information regarding microphysical structure of this cloud, but analysis of Z_{DR} signature can give some insights. In the lower panel of Fig. 2, there are “pockets” of high Z_{DR} (nearly 3 dB) located in regions with reflectivities about 20 dBZ. These regions of high Z_{DR} indicate ice crystal growth and changes of their growth regimes.

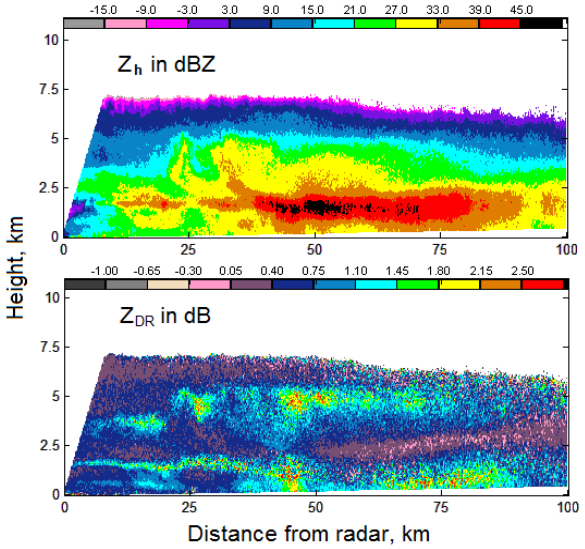

Fig.2. RHI of Z_{DR} and Z_h at the azimuth of 181° measured by KOUN radar on January 27, 2009, at 2317 UTC.

For quantitative analysis of observed polarimetric variables, vertical profiles through "pockets" of enhanced Z_{DR} at several distances from radar have been made. Profiles are made at 27, 45 and 50 km, and they have different maximum values but their shape is similar. Fig. 3, represents the vertical profile at 45 km distance from the radar.

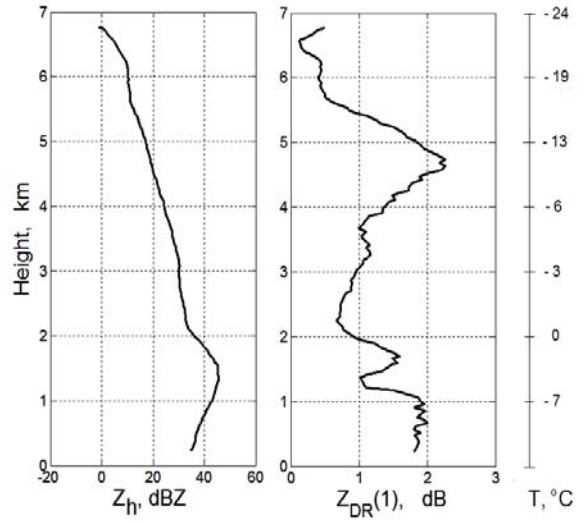

Fig.3. Vertical profile of Z_h and Z_{DR} made through the "pocket" of enhanced Z_{DR} at 45 km from radar; vertical profile of temperature from sounding is shown in the right scale.

From the cloud top (near 7 km) to melting layer (~2 km), Z_h gradually increases due to crystals' growth. Z_h reaches values of 30 dBZ right above the melting layer. Z_{DR} increases from the cloud top, where values are close to 0.5 dB, than increases abruptly reaching maximum value of 2.3 dB at 4.6 km. Based on measured temperature range (-16°C to -10°C), expected crystal habit at this height is dendritic (Bailey and Hallett 2008, Korolev 2000). According to observations done by Korolev et al. 2000, maximum frequency of occurrence of dendrites was observed in the temperature interval -15 ºC < T < -10 ºC, which is consistent with laboratory results (e.g. Hallett and Mason 1958, Magono and Lee 1966). Also, Korolev (2000) found that dendritic ice particles occur in isolated cells embedded in zones of irregular shaped ice particles that can reach fraction of 100% in those cells. However, there are cases where (in this temperature range) dominant crystal habit is irregular instead of dendrites.

After Z_{DR} reaches maximum, it begins to decrease rapidly due to aggregation which dominates at altitudes below 4.6 km. At this level, temperature is approximately -10°C, which is favorable for significant aggregation (Rodgers 1989). As aggregates grow, they become more spherical in shape and their density decreases. Low density of this crystal habits affects dielectric constant which becomes smaller compared to dielectric constant of solid ice. Thus, Z_{DR} decreases to values less than unity in Figure 3, or nearly zero in other vertical profiles (not shown). Given the observed low values of Z_{DR} in regions of aggregates, it is expected that these hydrometeors would have roughly spherical shape, so their aspect ratio would be close to unity. Aggregates of dendritic crystals tend to become large and typical diameter is between 2 and 5 mm. Aggregates have low density and they are more spherical in shape compare to pristine plate crystals. Formation of aggregates will cause increase in Z_h and decrease in Z_{DR} value. This process is dominant at lower temperatures (-15ºC) and high ice crystal concentrations. Below 4.6 km Z_h is still increasing, due to large size of aggregates (values exceed 30 dBZ).

The focus of our study is the radar fields above the melting layer (>2 km) and the explanation of enhanced Z_{DR} signature in terms of processes that may have lead to this signature. We hypothesize that increase in Z_{DR} is related to regions of "embedded convection" containing small supercooled droplets which can not be detected by radar. However, it is possible to detect the consequence of their presence. Within "pockets" of enhanced Z_{DR}, in terms of liquid water content, conditions are slightly different compared to the

rest of the cloud above the melting layer. Using model output we are trying to replicate the observed Z_{DR} signature and determine which crystal habit contributes the most to the observed Z_{DR} signature. Presence of supercooled droplets of various sizes would induce rapid ice crystals growth within the region of embedded convection. We assume that crystals grow rapidly by deposition due to the flux of water vapor from the drops to the crystal, producing high Z_{DR}.

3. ONE DIMENSIONAL MICROPHYSICAL MODEL

To replicate the observed Z_{DR} signature, we used an output from a simple 1D bulk microphysical model. The model takes the sounding from OUN 28 January 2009 at 00 UTC as an input. Based on the temperature and saturation profile from sounding along with the habit diagram from Bailey and Hallett (2008), the following crystal habits have been chosen: stellar dendrites, columns, plates and snow aggregates. Fig. 5 represents the habit diagram, obtained from laboratory results and pictures from cloud particle imager (CPI). Unlike Magono and Lee (1966), new diagram emphasizes that most ice crystals are irregular in shape and are mostly polycrystalline at temperatures below -20ºC.
The model includes nucleation process (activation of ice nuclei to form ice crystals within ice supersaturation conditions), deposition (diffusion of water vapor to a crystal) and aggregation (process of collision and coalescence that produce clusters of ice crystals).

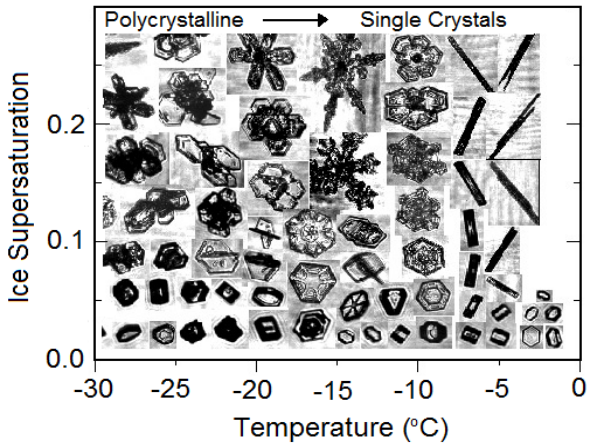

Fig.5. Habit diagram in pictorial format for atmospheric ice crystals adapted from Bailey and Hallett, 2008.

In calculations of radar variables, plates and dendrites are parameterized as oblate spheroids, columns and snow aggregates are represented as prolate spheroids and spheres, respectively. Particle size distribution is parameterized in a form of the exponential distribution. Density of dendrites and snow aggregates is calculated using power low relation between density (ρ) and diameter (D), as given in Cotton et al. 1986:

$$\rho = 43.5D^{-0.377} \tag{3.1}$$

$$\rho = 0.94644D^{-0.6} \tag{3.2}$$

Columns and plates have density of solid ice (0.92 g cm^{-3}). Aspect ratio is given as ratio of thickness and diameter of ice crystals, except for snow aggregates. Because of complexity of snow aggregate shape we used two constant values of aspect ratio 0.6 and 0.8 as did Matrosov et al. 1996. Korolev (2000) has found that roundness is a function of particle size but not temperature. For particles within the range of 60 to 1000 μm, the aspect ratio, on the other hand, is mainly a function of temperature but not the particle's size. For temperature range from 0ºC to -20ºC, the aspect ratio is about 0.6 with very small deviations about this mean value.

To calculate Z_h and Z_{DR}, the following model output is used: equivalent volume diameter, characteristic diameter and thickness of crystals, density for each crystal habit, and size distribution parameters (the intercept and slope parameter). The scattering amplitudes, $f_{,b,}$ were calculated in the Rayleigh approximation:

$$f_{a,b} = \frac{\pi^2 D^3}{6\lambda^2} \frac{1}{L_{a,b} + \frac{1}{\varepsilon_s - 1}} \tag{3.3}$$

where λ is the radar wavelength, $D = (ab^2)^{1/3}$ is the equivalent volume diameter of the particle (a is the vertical and *b* is horizontal axis), $L_{a,b}$ is the shape parameter, and ε_s is the dielectric constant for snow given as:

$$\varepsilon_s = \frac{1 + 2\frac{\rho_s}{\rho_i}\frac{\varepsilon_i - 1}{\varepsilon_i + 2}}{1 - \frac{\rho_s}{\rho_i}\frac{\varepsilon_i - 1}{\varepsilon_i + 2}} \tag{3.4}$$

Density of solid ice is denoted with ρ_i and density of snow is denoted as ρ_s which is the model output, and ε_i is the dielectric constant of solid ice. The shape parameters L_a and L_b are defined as:

$$L_a = \frac{1+f^2}{f^2}\left(1-\frac{\operatorname{arctg} f}{f}\right), \quad f=\sqrt{\frac{b^2}{a^2}-1}, \qquad L_b = \frac{1-L_a}{2} \tag{3.5}$$

for oblate crystals (dendrites and plates), and for prolate crystals (columns), they are:

$$L_a = \frac{1-e^2}{e^2}\left(\frac{1}{2e}\ln\left(\frac{1-e}{1+e}\right)-1\right), \quad e=\sqrt{1-\frac{b^2}{a^2}}, \qquad L_b = \frac{1-L_a}{2} \tag{3.6}$$

Z_h, Z_v and Z_{DR} are calculated using an exponential size distribution and the following equations:

$$Z_h = \frac{4\lambda^4}{\pi^4 |K_i|^2}\sum_{i=1}^{M}\int_{\infty}^{0}\left\{|f_{bi}|^2 - 2\,\mathrm{Re}\left[f^*_{bi}\left(f_{bi}-f_{ai}\right)\right]A_{2i} + |f_{bi}-f_{ai}|^2 A_{4i}\right\} N_i(D)\,dD \tag{3.7}$$

$$Z_v = \frac{4\lambda^4}{\pi^4 |K_i|^2}\sum_{i=1}^{M}\int_{\infty}^{0}\left\{|f_{bi}|^2 - 2\,\mathrm{Re}\left[f^*_{bi}\left(f_{bi}-f_{ai}\right)\right]A_{1i} + |f_{bi}-f_{ai}|^2 A_{3i}\right\} N_i(D)\,dD \tag{3.8}$$

$$Z_{dr} = \frac{Z_h}{Z_v}, \quad Z_{DR} = 10\log\left(Z_{dr}\right) \tag{3.9}$$

K_i for ice is 0.21, and $A_{1,2,3,4}$ are angular moments. We assume that particles are horizontally oriented in the mean but experience fluctuations in orientations. Changes in orientations of ice particles are important for Z_{DR}. To model such fluctuations, a two-dimensional axisymmetric Gaussian distribution of orientation is used for dendrites, plates and snow aggregates (Ryzhkov et al., 2009). For columns, we have used random orientation in the horizontal plane (Ryzhkov et al., 2009).

Angular moments for random orientation in the horizontal plane are defined as:

$$A_1 = \frac{1}{2}\sin^2\beta, \quad A_2 = \frac{1}{2}, \quad A_3 = \frac{3}{8}\sin^2\beta, \quad A_4 = \frac{3}{8}, \quad A_5 = \frac{1}{8}\sin^2\beta \tag{3.10}$$

where β represents elevation angle. Angular moments for two-dimensional axisymmetric Gaussian distribution of orientations are:

$$A_1 = \frac{1}{4}(1+r)^2, \quad A_2 = \frac{1}{4}\left(1-r^2\right), \quad A_3 = \left(\frac{3}{8}+\frac{1}{2}r+\frac{1}{8}r^4\right)^2, \quad A_4 = \left(\frac{3}{8}-\frac{1}{2}r+\frac{1}{8}r^4\right)\left(\frac{3}{8}+\frac{1}{2}r+\frac{1}{8}r^4\right), \quad A_5 = \frac{1}{8}\left(\frac{3}{8}+\frac{1}{2}r+\frac{1}{8}r^4\right)\left(1-r^4\right), \quad r = \exp\left(-2\sigma^2\right) \tag{3.11}$$

where σ represents the width of canting angle distribution. For σ equal zero, particles are oriented horizontally. For simplicity we used the same and constant value of 35° for σ for each crystal habit. Values of Z_{DR} for ice crystals are significantly higher if their change in orientations is not included.

4. RESULTS

Figs. 6 and 7 represent the calculated Z_h and Z_{DR} for each crystal habit separately, along with the bulk Z_h and the bulk Z_{DR}. The radar variables have been calculated using the microphysical model outputs. As already stated, melting layer is not addressed, thus signature below 2 km in both figures, should be disregarded. From figure 6 one can see that the bulk Z_h values are nearly 30 dBZ at approximately 4.5 km of height which coincide with the observed values. Considering Z_h contributions from different crystal habits, we conclude that the largest contribution comes from plates. Dendrites, columns and snow aggregates have Z_h close to 0 dB at this height, indicating negligible contribution.

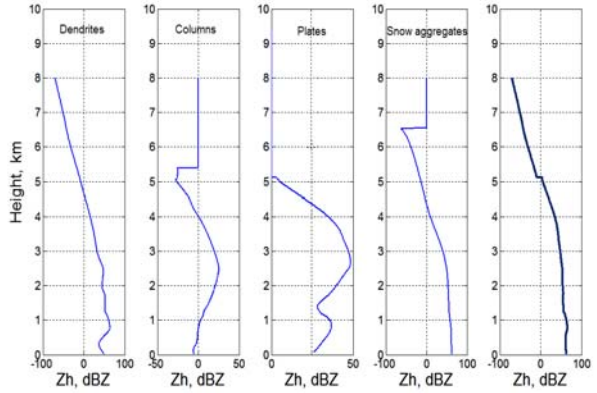

Fig.6. Calculated Z_h for each crystal habit separately (first 4 panels) and the bulk Z_h (the last panel on the right)

From figure 7, we see that plates have significant influence on the bulk Z_{DR}, as expected. Values at the top of the area with enhanced Z_{DR} (values are little more than 1 dB) are due to dendrites. At lower heights, a small decrease in Z_{DR} is caused by snow aggregates. Sharp increase and maximum ($Z_{DR} \approx 2.3$ dB) is located at level where plates appear. At lower part of the area with enhanced Z_{DR} there is decrease in Z_{DR} (close to 0 dB) due to snow aggregates with significantly lower density. Nearly constant Z_{DR} signature (~3.5 dB) for columns is due to the almost constant aspect ratio, meaning that particles grow in such a way that the ratio between vertical and horizontal axis remains almost the same. This also applies to plates that have Z_{DR} near 2.3 dB. In case of snow aggregates, Z_{DR} has the lowest value (~0.08 dB), and is constant, because the aspect ratio is chosen to be 0.6.

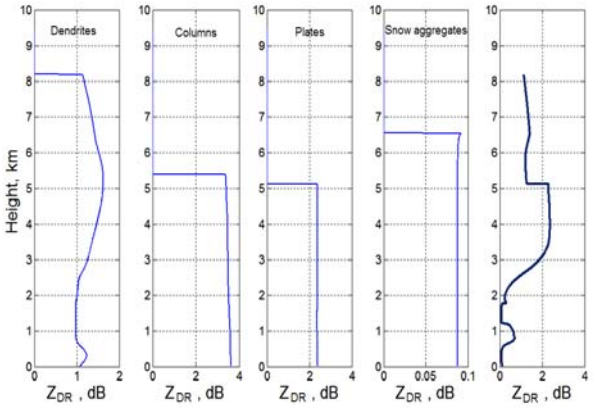

Fig.7. Calculated Z_{DR} for each crystal habit separately (first 4 panels) and the bulk Z_{DR} (the last panel on the right)

Changes in particles' orientations significantly affect the polarimetric variables. In case σ = 0, calculated Z_{DR} have larger values (up to 8 dB for plates). For columns, random distribution in horizontal plane has been used and their Z_{DR} depends on the elevation angle only. So, we had limited influence on orientation of columns.
We conclude that the 1D microphysical model captures the essential features of the profiles of reflectivity and differential reflectivity which observed with the S-band polarimetric radar.

5. CONCLUSION

Radar observations with the dual-polarization S-band WSR-88D radar in stratiform precipitation and clouds frequently exhibit areas of enhanced Z_{DR}, above the melting layer, i.e., at subfreezing temperatures. Measured interval of Z_{DR} values from 0 to 2.5 dB signifies presence of large horizontally oriented ice particles. The areas of enhanced Z_{DR} are observed in forms of layers or "pockets" indicating significant spatial variations in microphysical and dynamical processes in clouds.

We made an attempt to replicate vertical profiles of measured radar reflectivity and Z_{DR} using a simple 1D microphysical model output. The model includes four types of ice crystal particles: dendrites, plates, columns, and snow aggregates. The first three habits grow by deposition of water vapor and aggregation, whereas snow aggregates are mainly formed by aggregation. The ambient atmospheric parameters used for the model input have been obtained from rawinsonde sounding, conducted at the time of radar observations. The output parameters from the model are number concentrations of the ice habits, sizes and density of ice particles. To calculate radar variables, we approximated ice dendrites and plates with oblate spheroids, columns were approximated with prolate spheroids, and the aggregates were considered as spheres. Changes of particles' orientations are also included in calculation of radar variables.

We were able to reproduce the radar profile of reflectivity, Z_h, and local enhancement in Z_{DR} above the melting layer. Despite the presence of local maximums in Z_h contributions from different particles' habits, the bulk Z_h profile is smooth and replicates the radar one nicely. Z_{DR} profile obtained from the model reproduces the main features of the measured radar profile. The strongest contribution to enhanced Z_{DR} comes from dendrites although the transition to the

enhanced Z_{DR} is rather sharp. Further decrease in Z_{DR} toward the ground is explained with aggregation process. Good agreement between the observed radar profiles and the calculated ones demonstrates acceptable accuracy of the model.

6. REFERENCES

Bailey, M. P. and J. Hallett, 2009: A comprehensive habit diagram for atmospheric ice crystals: Conformation from the laboratory, AIRS II, and other field studies. *J. Atmos. Sci.*, **66**:2888–2899

Cotton W. R., G. J. Tripoli, R. M. Rauber, and E. A. Mulvihill, 1986: Numerical simulation of the effects of varying ice crystal nucleation rates and aggregation processes on orographic snowfall. J. Climate Appl. Meteor., **25**, 1658-1680.

Doviak, R. J. and D. S. Zrnic, 1993: Doppler radar and weather observations, 2nd ed., Dover Publications, 562 pp.

Ikeda, K., E.A. Brandes, and R.M. Rasmussen, 2005: Polarimetric Radar Observation of Multiple Freezing Levels. *J. Atmos. Sci.*, **62**, 3624–3636.

Istok, M., M. Fresch, Z. Jing, S. Smith, R. Murnan, A. Ryzhkov, J. Krause, M. Jain, P. Schlatter, J. Ferree, B. Klein, D. Stein, G. Cate, R. Saffle, 2009: WSR-88D dual-polarization initial operational capabilities. *25*th *Conf. on IIPS, Amer. Meteorol. Soc*., Phoenix, AZ, 15.6.

Hogan R. J., P. R. Field, A. J. Illingworth, R. J. Cotton and T. W. Choularton, 2002: Properties of embedded convection in warm-frontal mixed-phase cloud from aircraft and polarimetric radar. *Q.J.R. Met. Soc*., **128**, pp. 451-476.

Korolev, A.V., G.A. Isaac and J. Hallett, 2000: Ice particle habits in stratiform clouds. *Quart.J.R. Met. Soc.*, **126**, 2873-2902.

Korolev, A., and G. Isaac, 2003: Roundness and Aspect Ratio of Particles in Ice Clouds. *J. Atmos. Sci.*, **60**, 1795–1808.

Magono, C. and C.W. Lee, 1966: Meteorological classification of natural snow crystals. *Jour.Fac. Sci., Hokkaido* Univ. Series VII, **2**, 321-335.

Matrosov, S.Y., R.F. Reinking, R.A. Kropfli, and B.W. Bartram, 1996: Estimation of Ice Hydrometeor Types and Shapes from Radar Polarization Measurements. *J. Atmos. Oceanic Technol.*, **13**, 85–96.

Matrosov, S. Y., R.F. Reinking, R.A. Kropfli, B. E. Martner, and B.W. Bartram, 2001: On the use of radar depolarization ratios for estimating shapes of ice hydrometeors in winter clouds. *J. Applied Meteorol.*, **40**, 479-490.

Melnikov, V.M., and D.S. Zrnić, 2007: Autocorrelation and Cross-Correlation Estimators of Polarimetric Variables. *J. Atmos. Oceanic Technol.*, **24**, 1337–1350.

Pruppacher, H. R. and J. D. Klett, 1980: *Microphysics of Clouds and Precipitation*. D. Reidel, 508pp.

Passarelli, R. E., 1978: Theoretical and Observational Study of Snow-Size Spectra and Snowflake Aggregation Efficiencies. *J. Atmos. Sci.*, **35**, 882–889.

Reinking, R. F., S. Y. Matrosov, R. A. Kropfli, and B.W. Bartram, 2002: Evaluation of a 45-slant quasi-linear radar polarization state for distinguishing drizzle droplets, pristine ice crystals, and less regular ice particles. *J. Atmos. Oceanic Technol.*, **19**, 296-321.

Rogers, R.R. and M.K. Yau., 1989: *A Short Course in Cloud Physics*, 3rd. ed. Elsevier Press, 160 pp

Ryzhkov, A. V., Pinsky A., Khain A., 2009: Polarimetric radar observation operator for a cloud model with spectral microphysics. Submitted to the *J.Atmos. Sci.*

Zrnic D.S., V. M. Melnikov, and J. K. Carter, 2006: Calibrating differential reflectivity on the WSR-88D. *J. Atmos. Ocean. Technol*., **23**, 944-951.